Ether- versus Ester-Linked Phospholipid Bilayers Containing either Linear or Branched Apolar Chains

ARTICLE *in* BIOPHYSICAL JOURNAL · SEPTEMBER 2014

Impact Factor: 3.97 · DOI: 10.1016/j.bpj.2014.07.036 · Source: PubMed

5 AUTHORS, INCLUDING:

Daniel Balleza
Italian National Research Council
16 PUBLICATIONS **30** CITATIONS
SEE PROFILE

Kepa Ruiz-Mirazo
Universidad del País Vasco / Euskal Herriko …
48 PUBLICATIONS **658** CITATIONS
SEE PROFILE

Article

Ether- versus Ester-Linked Phospholipid Bilayers Containing either Linear or Branched Apolar Chains

Daniel Balleza,[1,2] Aritz B. Garcia-Arribas,[1,2] Jesús Sot,[1,2] Kepa Ruiz-Mirazo,[1,3] and Félix M. Goñi[1,2,*]
[1]Unidad de Biofísica CSIC, UPV/EHU and [2]Departamento de Bioquímica, Universidad del País Vasco, Leioa, Spain; and [3]Departamento de Lógica y Filosofía de la Ciencia, UPV/EHU, Donostia-San Sebastián, Spain

ABSTRACT We studied the properties of bilayers formed by ether-and ester-containing phospholipids, whose hydrocarbon chains can be either linear or branched, using *sn*-1,2 dipalmitoyl, dihexadecyl, diphytanoyl, and diphytanyl phosphatidylcholines (DPPC, DHPC, DPhoPC, and DPhPC, respectively) either pure or in binary mixtures. Differential scanning calorimetry and confocal fluorescence microscopy of giant unilamellar vesicles concurred in showing that equimolar mixtures of linear and branched lipids gave rise to gel/fluid phase coexistence at room temperature. Mixtures containing DHPC evolved in time (0.5 h) from initial reticulated domains to extended solid ones when an equilibrium was achieved. The nanomechanical properties of supported planar bilayers formed by each of the four lipids studied by atomic force microscopy revealed average breakdown forces F_b decreasing in the order DHPC $\geq$ DPPC $>$ DPhoPC $>>$ DPhPC. Moreover, except for DPPC, two different F_b values were found for each lipid. Atomic force microscopy imaging of DHPC was peculiar in showing two coexisting phases of different heights, probably corresponding to an interdigitated gel phase that gradually transformed, over a period of 0.5 h, into a regular tilted gel phase. Permeability to nonelectrolytes showed that linear-chain phospholipids allowed a higher rate of solute + water diffusion than branched-chain phospholipids, yet the former supported a smaller extent of swelling of the corresponding vesicles. Ether or ester bonds appeared to have only a minor effect on permeability.

INTRODUCTION

Biological membranes perform the important function of delimiting the cytosol from the external, aqueous milieu without taking those two different chemical domains apart, and instead fostering a strong and highly regulated interaction between them. In this context, it is remarkable that the membrane phospholipids of *Archaea*, the third domain of life, have a distinct molecular nature compared with those found in *Bacteria* and *Eukarya* (1). First, the hydrophobic tails in archaebacterial lipids are typically polyprenyl saturated chains containing methyl branches, whereas their bacterial and eukaryotic counterparts are composed of mostly linear fatty acids in the range of C12–C24, with varying degrees of saturation, isomer conformation, and occasional cyclization and branching (2). Second, *Archaea* membranes are rich in di- and tetraether lipids, in contrast to the ester-linked conventional mesophilic lipids in bacteria and eukaryotes (3,4).

The phytanyl (3, 7, 11, 15-tetramethylhexadecyl) lipid moiety is broadly known from studies on extremophiles and *Archaea* to form stable membranes under extreme habitats such as hot springs, salt lakes, and acidic spots (5,6). Synthetic *Archaea*-like lipids have also been studied in some detail. For instance, diphytanoyl phosphorylcholine (ester-DPhoPC) was shown to promote high bilayer stability and low ionic permeability (7,8), high viscoelasticity (probably derived from its ability to imbibe plenty of water molecules), and restricted rotational and lateral diffusive motions but significant headgroup mobility (9,10). In turn, diphytanyl phosphocholine (ether-DPhPC) was reported to be highly stable, salt tolerant, and proton impermeable (11–14). Moreover, it is well known that ether-bound phytanyl lipids are chemically more stable than the ester-bound ones (15).

Recent studies include two important related contributions: one compared the ether versus ester linkage (in 1,2-di-O-hexadecyl-*sn*-glycero-3-phosphocholine (DHPC) and 1,2-dipalmitoyl-*sn*-glycero-3-phosphocholine (DPPC), respectively) (16), and the other described the structure and water permeability of the isoprenoid (branched) DPhoPC (17). In this study, we built on those two publications by comparing the properties of phosphatidylcholines (PCs) containing ester- and ether-linked, linear and branched alkyl chains. For this purpose, we evaluated the thermotropic phase behavior, interfacial properties, formation of lipidic domains in giant unilamellar vesicles (GUVs), and nonelectrolyte permeabilities of such lipids. Hence, we employed liposomes composed of ester-DPhoPC, ether-DPhPC, ester-DPPC, or ether-DHPC, either pure or in binary mixtures. The stereostructure of the glycerol backbone in the phospholipids of *Bacteria* and *Eukarya* is *sn*-glycerol-3-phosphate (*sn*-G3P), whereas in the polar lipids of *Archaea* it is *sn*-glycerol-1-phosphate (*sn*-G1P) (6). However, in this work we employed synthetic analogs (*sn*-G3P), so stereochemical

Submitted March 28, 2014, and accepted for publication July 15, 2014.

*Correspondence: felix.goni@ehu.es

Editor: Claudia Steinem.

0006-3495/14/09/1364/11 $2.00

http://dx.doi.org/10.1016/j.bpj.2014.07.036

effects were excluded. The chemical structures of the phospholipids and nonelectrolytes used are depicted in Scheme 1. Our study reveals peculiarities of the ester and ether lipids, including their different bilayer phase behaviors. Greater differences are found between bilayers formed by the linear and branched lipids in terms of their nanomechanical properties (breakdown forces) and permeability to nonelectrolytes.

MATERIALS AND METHODS

Sample preparation

All lipids were purchased from Avanti Polar Lipids (Alabaster, AL) and used without further purification. We obtained 2-dimethylamino-6-lauroylnaphthalene (Laurdan) and 1-(4-trimethylammoniumphenyl)-6-phenyl-1,3,5-hexatriene *p*-toluenesulfonate (TMA-DPH) from Molecular Probes (Alabaster, AL). We prepared phospholipid multilamellar vesicles (MLVs) by dissolving each phospholipid in chloroform/methanol (2:1), mixing them in the appropriate proportions (binary mixtures at 1:1 ratios were typically used), and drying the samples for 2 h under vacuum. The dry lipids were resuspended in a PIPES-EDTA or choline chloride buffer (depending on the type of measurement to be carried out (calorimetry or spectrophotometry); see details below) at 65°C, well above all lipid transition temperatures, for ~20 min (gentle mixing was applied to favor vesicle formation). The samples were then allowed to cool down to room temperature (or ~10°C for differential scanning calorimetry (DSC)).

DSC

We observed the phase transitions of phospholipid bilayer vesicles under 24 psi pressure using a VP-DSC high-sensitivity differential scanning calorimeter (MicroCal, Northhampton, MA). Measurements were carried out in 20 mM PIPES, 150 mM NaCl, 1 mM EDTA, pH 7.4 buffer. Vesicle solutions were prepared at 1.0 or 2.0 mmol L^{-1}. The heating rate was 45°C/h. Thermograms were recorded after sample equilibration at the starting temperature. We performed buffer subtraction, baseline correction, and integration of the calorimetric endotherms using the Microcal Origin software.

Fluorescence spectroscopy

Fluorescence spectroscopy was performed in a PTI-MP1 spectrofluorometer (Photon Technology International) equipped with a thermoregulated cell holder for measurements at 20°C and 45°C, and with polarizers for the anisotropy of TMA-DPH fluorescence.

The Laurdan generalized polarization excitation (GP_{EX}) parameter was calculated according to

$$GP_{EX} = (I_{440}\text{-}I_{490})/(I_{440} + I_{490})$$

where I_{440} and I_{490} are the emission intensities obtained at 440 and 490 nm, respectively, with excitation at 360 nm. The final probe/lipid molar ratio was 1:500.

For anisotropy of TMA-DPH fluorescence measurements, the instrument software computes anisotropies from the averages of ten measurements for each experimental point, correcting for the G factor. TMA-DPH fluorescence was excited at 360 nm and emission was recorded at 430 nm. The final probe/lipid molar ratio was 1:250. To avoid light scattering and inner filter effects, fluorescence anisotropy was measured on increasingly diluted samples. Only when anisotropy values remained constant with further dilution were they recorded.

Supported planar bilayer preparation

Supported planar bilayers (SPBs) were prepared on high-quality, V-2 grade, scratch-free mica substrates (Asheville-Schoonmaker Mica, Newport News, VA) that were previously attached to round 24 mm glass coverslips with the use of a two-component optical epoxy resin (EPO-TEK 301-2FL; Epoxy Technology, Billerica, MA). SPBs were prepared according to the vesicle adsorption method (18). For this purpose, multilamellar vesicles (MLVs) were initially prepared by mixing the appropriate amounts of synthetic pure lipids in chloroform/methanol (2:1, v/v) solutions. Samples were then dried by evaporating the solvent under a stream of nitrogen and placing them into high vacuum for 2 h. The samples were then hydrated in assay buffer and highly vortexed at a temperature above that of the sample lipids' highest phase transition. After the lipids became completely detached from the test-tube bottom, the formed MLVs were introduced into a FB-15049 (Fisher Scientific, Waltham, MA) bath sonicator and kept at 60°C for 1 h. In this way, a proportion of small unilamellar vesicles (SUVs) were generated. Then, 120 μl of assay buffer containing 3 mM $CaCl_2$ was added onto a previously prepared 1.2 cm^2 freshly cleaved mica substrate mounted onto a BioCell coverslip-based liquid cell for atomic force microscopy (AFM) measurements (JPK Instruments, Berlin, Germany). Then, 60 μl of the sonicated vesicles was added on top of the mica. Final lipid concentration was 150 μM. Vesicles were left to adsorb and extend for 30 min maintaining the sample temperature at 70°C. The samples were left to equilibrate at room temperature for 30 min, and then the nonadsorbed vesicles were discarded by washing the samples 10 times with assay buffer in

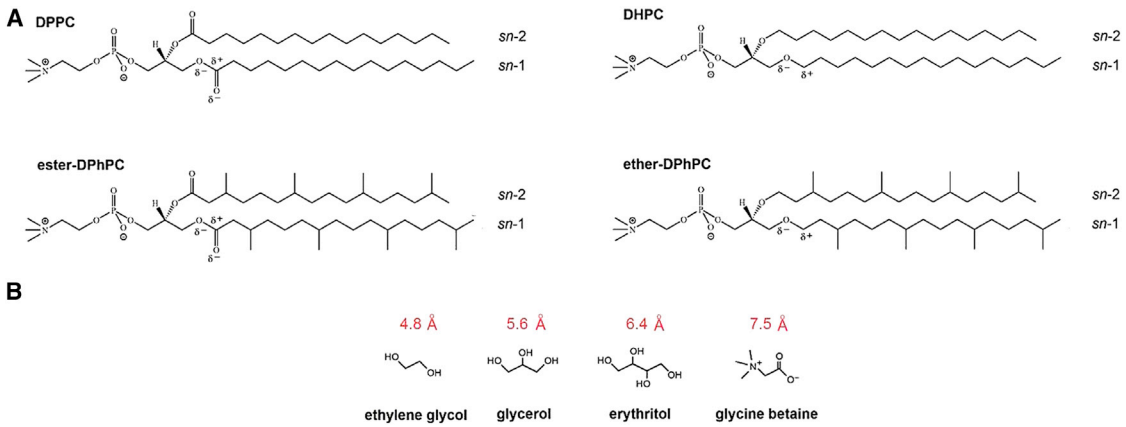

SCHEME 1 (*A* and *B*) Chemical structures of (*A*) DPPC, DHPC, DPhoPC, and DPhPC (images from Avanti Polar Lipids), and (*B*) the nonelectrolytes employed in our permeability assays (e-glycol, glycerol, erythritol), and glycine-betaine.

the absence of $CaCl_2$. A small amount of buffer was always left on top of the substrate to keep the SPBs hydrated at all times. The BioCell was set to 23°C and the planar bilayers were left to equilibrate for 1 h prior to AFM measurements.

AFM imaging

Planar bilayer topography was performed under contact-mode AFM scanning (constant vertical deflection) in a NanoWizard II AFM (JPK Instruments, Berlin, Germany). For proper measurements, the AFM was coupled to a Leica microscope and mounted onto a Halcyonics Micro 40 antivibration table (Halcyonics, Menlo Park, CA) and inside an acoustic enclosure (JPK Instruments). The Biocell liquid sample holder (JPK Instruments) was used to control the assay temperature at 23°C. V-shaped MLCT Si_3N_4 cantilevers (Veeco, Plainview, NY) with nominal spring constants of 0.1 N/m were used for bilayer imaging, always keeping the minimum possible force. Then, 512 × 512 pixel resolution images were collected at a scanning rate of 1 Hz and line fitted using the JPK Data Processing software.

Force spectroscopy

Before imaging, V-shaped MLCT Si_3N_4 cantilevers (Veeco, Plainview, NY) with nominal spring constants of 0.1 N/m were individually calibrated in a lipid-free mica substrate in assay buffer using the thermal-noise method. After proper AFM imaging to check for correct lipid extension of the SPBs, force spectroscopy was performed at a speed of 1 μm/s in not less than 500 × 500 nm bilayer areas in the form of 10 × 10 or 15 × 15 grids. Force curves were batch analyzed with JPK Data Processing software and bilayer breakthrough events were determined for each of the indentation curves as reproducible force steps or jumps within the extended traces. Histograms were generated from at least three independent sample preparations with at least three independently calibrated cantilevers (n = 647–2767).

Preparation of GUVs

GUVs were prepared at 65°C according to the electroformation method (19) with small modifications. Pure lipids and mixtures were suspended in chloroform/methanol (2:1, v/v) and GUVs were prepared using 10 mM Tris, pH 7, as buffer. Stock solutions of lipids (0.2 mg/ml total lipid containing 0.2% DiI or Rhodamine-DOPE) were transferred to Pt wires and connected to an electric wave generator under AC field conditions (frequency, 500 Hz; amplitude, 5.3 Vp-p) for 1.5 h at 65°C. The GUVs were then observed on an inverted confocal fluorescence microscope at 20°C.

Permeability measurements

All permeability measurements were performed at 20°C by spectrophotometry. MLVs (prepared at 2.5 mM in 50 mM choline chloride) were diluted (1:50 v/v) in a nonelectrolyte solution (100 mM) of glycol (62.07 $gmol^{-1}$), glycerol (92.09 $gmol^{-1}$), erythritol (122.12 $gmol^{-1}$), or glycine betaine (117.15 $gmol^{-1}$). The subsequent swelling of the vesicles and permeation of nonelectrolytes through the membrane caused a decrease in turbidity (A_{450}) that was measured as a function of time (20). The measurements are expressed as a normalized relative volume decrease, reflecting the entry of water and solutes into the vesicles and the consequent increase in translucency of the samples.

RESULTS

Thermotropic phase transitions

Fig. 1 shows representative DSC thermograms of the four phospholipids under study and their binary mixtures.

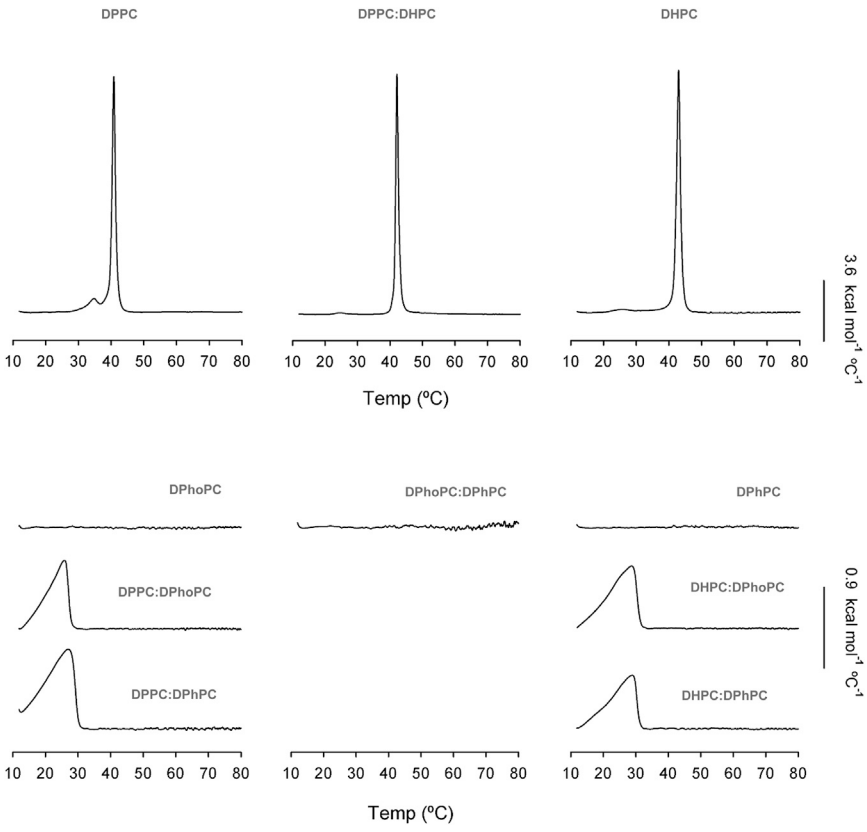

FIGURE 1 DSC thermograms of DPPC, DHPC, DPhoPC, DPhPC, and their binary mixtures. A heating rate of 45°C/h was used. The thermograms were recorded after sample equilibration at the starting temperature. The profiles correspond to heating scans.

The thermogram for pure DPPC, in agreement with previous reports, shows a small endotherm around 35°C (the pretransition temperature T_p) and a large endotherm at ~41.5°C (T_m). The first transition reflects a reorganization in the order of lipids in the membrane, in which the gel phase ($L_{\beta'}$) changes to a pseudo-melted rippled phase ($P_{\beta'}$), whereas beyond the T_m the liquid crystalline (L_α) phase is reached (21). The pure DHPC thermogram shows a very similar profile, with only slight differences. In the latter case, the pretransition was attributed to the change from an interdigitated gel phase ($L_{\beta I}$) to a $P_{\beta'}$ one (22). In our experimental setting, this transition takes place at ~26°C, whereas T_m occurs at 43°C (Fig. 1).

When DPhoPC or DPhPC were added to DPPC at equimolar ratios, the pretransition peak disappeared and the main transition peak became wider and asymmetric, and shifted toward lower temperatures (26–27°C). When the former lipids were mixed at the same equimolar ratios but with DHPC instead of DPPC, a similar effect was observed, with asymmetric main transitions at ~29°C. In contrast, when DPhoPC and DPhPC systems were employed, either pure or in an equimolecular mixture (Fig. 1), no detectable gel-to-liquid crystalline phase transition was registered over a broad temperature range (10–100°C).

Domain formation in mixed bilayers

We used the above-described lipid mixtures to prepare GUVs and study their possible segregation into well-defined domains by confocal fluorescence microscopy. Representative examples are shown in Fig. 2, corresponding to N-*Rh*-DOPE-labeled images taken at 20°C (~1 h after preparation, to allow sample cooling from formation temperature, $T = 65$°C). Independently of GUV size, which was somewhat variable (ranging from d = 5–10 μm up to 60 μm), fluid/solid phase coexistence was observed only in those mixtures in which asymmetric DSC thermograms were seen. Nevertheless, some interesting differences were detected in the process of phase separation. In binary mixtures containing DPPC (Fig. 2, *A* and *B*), lateral separation of dark and bright domains was clearly observed. However, when DHPC (ether linked) was used, finely reticulated domains appeared in the first minutes of observation (Fig. 2, *C* and *D*). These DHPC-specific reticulated domains were transient and disappeared soon (~20 min) after formation, allowing the formation of clearly separated dark and bright areas (Fig. 2, *E* and *F*). Since the large headgroup of rhodamine-DOPE hinders insertion into gel phases, it is assumed that these fluorescent molecules segregate into fluid domains (23). Hence, dark zones are most probably DPPC or DHPC rich. No phase separation was observed in mixtures that did not contain DPPC or DHPC (i.e., those that did not exhibit an endothermic signal in Fig. 1).

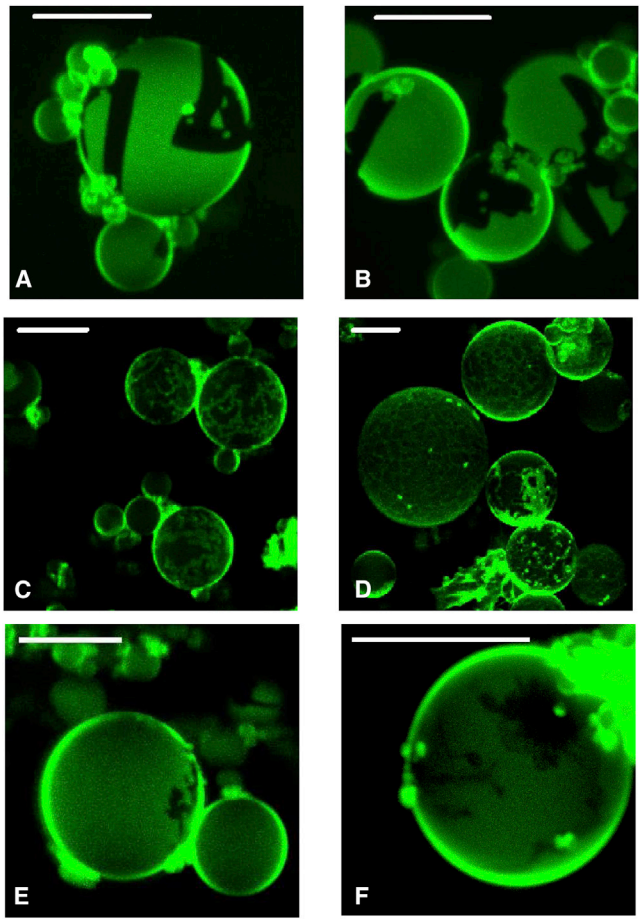

FIGURE 2 Micrographs of GUVs made of binary mixtures of linear and branched lipids: (*A*) DPhoPC/DPPC, (*B*) DPhPC/DPPC, (*C* and *E*) DPhoPC/DHPC, and (*D* and *F*) DPhPC/DHPC. DPPC and DHPC promote the formation of solid domains and a mixture of solid and reticulated coalescent domains, respectively. All scale bars are 10 μm. To see this figure in color, go online.

Fluorescent probes at the bilayer interfacial region

Further information on the properties of ether- versus ester-containing bilayers may be obtained with the use of fluorescent probes that are known to partition preferentially at the bilayer lipid/water interface. In particular, TMA-DPH and Laurdan have been used in bilayers formed by each of the four lipids under study. The values of the TMA-DPH anisotropies and Laurdan GPs obtained at 20°C and 45°C are shown in Fig. 3. The fluid-phase states at 20°C, according to the data in Figs. 1 and 2, are as follows: pure linear lipids, gel; pure branched lipids, fluid; linear/branched mixtures, gel/fluid coexistence; branched/branched mixture, fluid. At 45°C, all samples are in the fluid state. The measurements shown in Fig. 3 were made after a 5 min thermal equilibration, but preliminary experiments had shown no changes over a period of 25 min. TMA-DPH anisotropy reports on the molecular order at the interface (Fig. 3, *A* and *C*). As

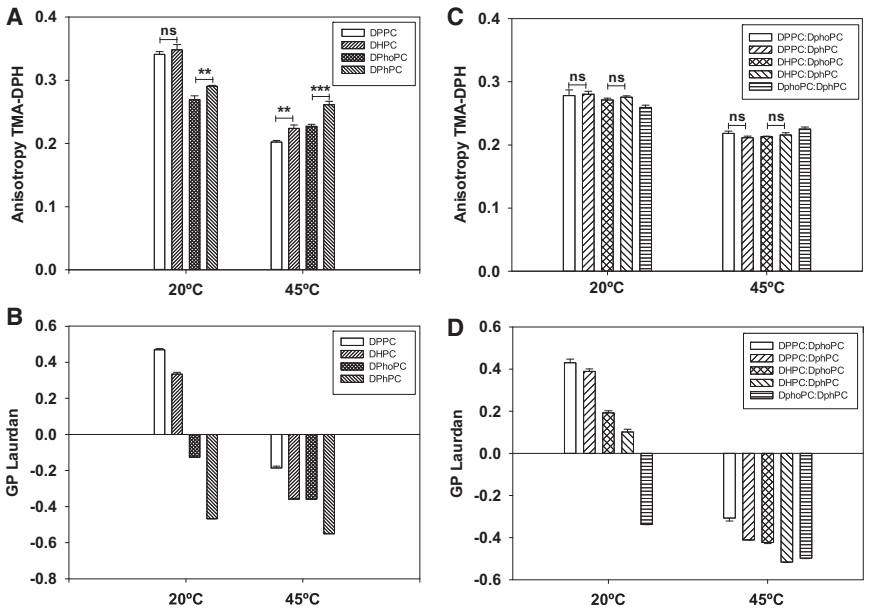

FIGURE 3 Fluorescence polarization data of bilayers (large unilamellar vesicles) composed of single phospholipids or binary mixtures. (*A* and *C*) TMA-DPH anisotropy. (*B* and *D*) Laurdan GP. Student's *t*-test of significance: $^{**}p < 0.005$; $^{***}p < 0.001$; n.s., nonsignificant.

expected, the order decreased when going from the low to the high temperature. It can also be seen that even if the differences are small, there is a higher degree of order for the ether than for the ester lipids, particularly at 45°C. For the binary mixtures (Fig. 3), these differences are blurred, and in general the anisotropy (molecular order) of the mixtures is lower than that of the pure components. Laurdan fluorescence relaxes through water dipoles. A low hydration in the region will mean poor relaxation and high GP values. When Laurdan GP is measured in our systems (Fig. 3, *B* and *D*), the results are consistent with the ether lipids being more hydrated than the ester lipids at their interfaces, and the branched ones being more hydrated than the linear ones. As expected from the lack of a detectable calorimetric transition for the branched lipids, their corresponding GP values are rather similar at 20°C and 45°C. In general, the binary mixtures (Fig. 3 *D*) reflect the combined properties of the components. The branched-chain mixture DPhoPC/DPhPC exhibits similarly low GP values (high hydration) at both temperatures.

AFM on SPBs

The SPBs that formed with each of the four lipids under study were examined by AFM in the force-spectroscopy mode. In this mode, the nanomechanical bilayers' resistance to piercing by the AFM tip is measured. Typically, the AFM-tip indentation process on planar bilayers provides a force-distance record with a 4–6 nm jump in the extension trace. This jump reflects the exact force at which tip penetration through the bilayers occurs and is known as the breakthrough force (F_b). Representative AFM-tip indentation curves are shown in Fig. 4. DPPC samples (Fig. 4, curve a) gave a single signal, with a jump at ~16 nN, similar to previously published values (24). However, for the other three lipids, two kinds of force curves were found in each case. Specifically, in a given SPB preparation, different indentation experiments provided either one or the other results (see, e.g., curves b and b′ for DHPC in Fig. 4). The alternative results were highly reproducible within each class. The statistics for the experiments on DPPC and DHPC are shown in Fig. 5. The two groups of results found with DHPC appear clearly separated in the histograms (Fig. 5 *B*), with F_b values of ~14 and 22 nN.

Bilayer breakthrough force histograms for branched-chain lipids are shown in Fig. 6. Two populations of F_b values are found for both DPhPC and DPhoPC; however, the forces are much lower for the ether (DPhPC; Fig. 6 *B*) than for the ester (DPhoPC; Fig. 6 *A*) lipid bilayers. The origin of this dual behavior is discussed below. The DPhoPC histogram is very similar to the one published by García-Manyes et al. (25) (DFPC in their nomenclature), but our F_b values are lower (by ~3 nN) than theirs, which we attribute to the different ionic composition of the buffer used. The same authors have shown that certain divalent cations, in particular Mg^{2+}, reinforce the nanomechanical resistance of lipid bilayers in SPB preparations.

In a different series of experiments, contact-mode AFM imaging was performed on DHPC SPBs. In contrast to the height-homogeneous extensions that are commonly found for DPPC (24), the DHPC bilayers had a heterogeneous appearance (Fig. 7 *A*), with two coexisting phases 3.8 and 5.7 nm in height, respectively (see histograms in Fig. 7 *E*). However, these two phases were not stable at 23°C and the lower one shrank with time, disappearing after ~30 min (Fig. 7, *A*, *D*, and *F*). This would be in agreement with the transient appearance of a reticulated phase in

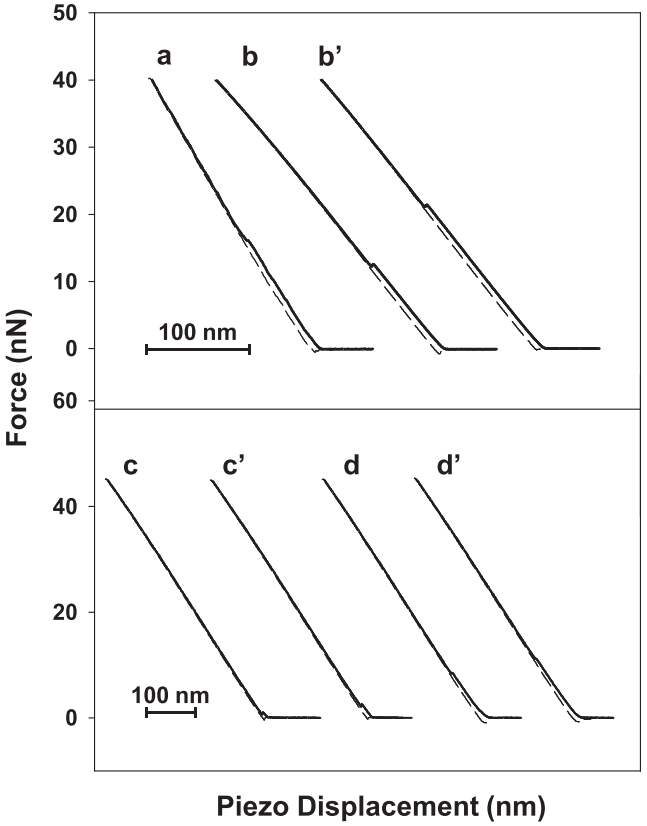

FIGURE 4 Representative AFM-tip indentation curves. Representative force curves from SPBs composed of DPPC (linear, ester) (a), DHPC (linear, ether) (b and b′), DPhPC (branched, ether) (c and c′), DPhoPC, (branched, ester) (d and d′). DHPC, DPhPC, and DPhoPC exhibit two alternative reproducible behaviors.

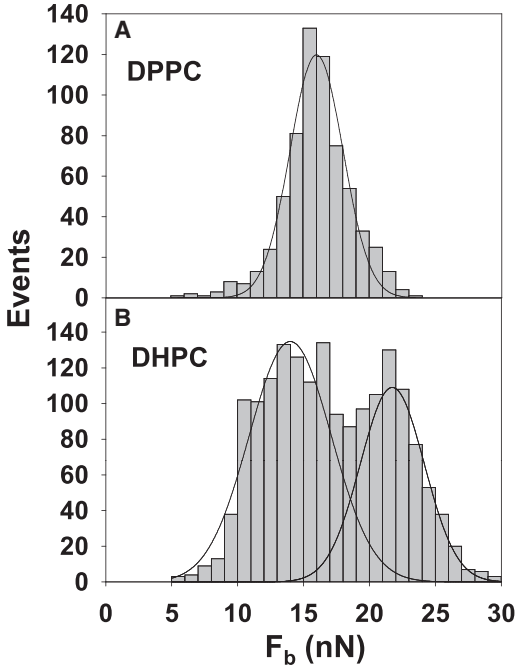

FIGURE 5 Bilayer breakthrough force (F_b) histograms of linear-chain lipids. The force step distribution from AFM-tip indentation curves on DPPC (*A*) (16.01 ± 2.01 nN, $n = 647$) and DHPC (*B*) (13.99 ± 3.13 nN and 21.74 ± 2.43 nN, $n = 1716$) is shown. Continuous lines represent Gaussian fittings. Each histogram is based on four samples analyzed with four different tips.

GUV made of mixtures containing DHPC (Fig. 2, *C–F*). In the light of studies by Guler et al. (16) and Maruyama et al. (22), it could be proposed that the lower phase corresponds to an interdigitated gel that is gradually transformed into a taller, tilted gel. The height of the tall DHPC phase is very similar to that of gel DPPC at 23°C (24). It appears that DHPC bilayers are not in equilibrium at 23°C, and this could explain the dual F_b values. Note that the TMA-DPH or Laurdan GP values of DHPC (or of DPPC) did not change with time in the first 30 min, as stated above. This is in agreement with changes taking place at the hydrophobic region of the bilayers (interdigitation) rather than those involving the lipid/water interface (e.g., gel-to-fluid phase transitions).

With respect to the dual F_b values found with DPhoPC and DPhPC, no time changes in AFM topography were seen. A possible explanation for this is that the lipid chain branching influences the piercing process so that there are two possible pathways for the tip. Alternatively, the SPB formed by branched-chain lipids could contain domains that are small and/or transient enough to be invisible in the AFM topographic images yet detectable by the force curves.

Assays for permeability to nonelectrolytes

To obtain a more complete picture of the properties of the bilayer membranes composed of these lipid mixtures, we tested the permeability of these membranes to nonelectrolytic compounds of various sizes: ethylene-glycol (e-glycol; 2-C), glycerol (3-C), and erythritol (4-C). In these experiments, the entry of water due to soluble diffusion inside the vesicles results in an increase of liposomal volume, which is measured through changes in turbidity. Because the mass of membrane lipids in each vesicle is constant but the volume is increased, the suspension turbidity decreases. Liposomes behave as ideal osmometers under these conditions (20). The time-dependent decrease in absorbance (A_{450}) was monitored and translated into relative volume changes, as shown in Fig. 8 for the most permeable species (e-glycol) in selected experiments at 20°C. At this temperature, DPPC forms a gel phase ($L_{\beta'}$), and consequently no e-glycol flux was observed with the pure lipid. However, when liposomes were heated above the T_m for this lipid (at 45°C), e-glycol permeation was detectable (Fig. 8, *A* and *G*). These results are consistent with the water permeability (P_f) reported for DPPC in gel (0.012×10^{-3} cm/s) and fluid (0.027 cm/s) phases, respectively (16).

The branched-chain lipids DPhPC and DPhoPC gave rise to bilayers that were clearly permeable to e-glycol

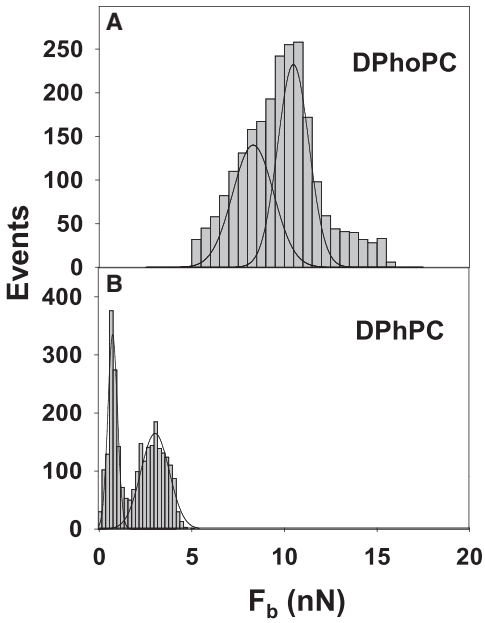

FIGURE 6 Bilayer breakthrough force (F_b) histograms of branched-chain lipids. The force step distribution from AFM-tip indentation curves from SPBs composed of DPhoPC (*A*) (8.31 ± 1.11 nN and 10.48 ± 0.84 nN, $n = 2279$) and DPhPC (*B*) (0.77 ± 0.26 nN and 3.06 ± 0.76 nN, $n = 2767$) is shown. Continuous lines represent Gaussian fittings. Each histogram is based on three samples analyzed with three different tips.

(Fig. 8, *D* and *E*), and the same was observed for equimolecular DPhPC/DPhoPC mixtures (Fig. 8 *F*; Table 1). Guler et al. (16) reported that water permeability for fluid-phase DHPC was slightly lower than that for DPPC, consistent with Nagle et al.'s (26) triple-slab theory. We measured e-glycol permeability at 48°C for the four lipids under study. The initial rates of vesicle volume change (i.e., solute + water entrance), τ, were 0.43 (DPPC), 0.34 (DHPC), 0.15 (DPhoPC), and 0.19 (DPhPC) (Table 1). Thus, our results confirm Nagle et al.'s predictions and observations for linear-chain lipids, but do not appear to do so for the branched-chain lipids.

DPhoPC and DPhPC in equimolar mixtures with DPPC show 1.6 and 2.4 times faster permeation rates than each pure lipid, respectively. Taking into account that these mixtures show formation of solid domains in GUVs (Fig. 2), the previous results indicate that permeation could be enhanced at the boundaries with disordered phases, rich in branched lipids. This is confirmed by the observations of mixtures containing DPPC (or DHPC) and a branched lipid at 45°C. In these cases, the permeability rates are similar to those of the linear lipid, DPPC or DHPC, at 45°C, showing that when the lipid mixture is in the fluid phase, lipid composition is less important for permeability. Glycerol and erythritol showed a qualitative behavior similar to that of e-glycol, although their permeation capacity was significantly lower due to their larger molecular masses (see, e.g., Fig. 8 *L*). In all of these experiments, glycine-betaine (GB), an N-trimethylated amino acid, was used as a control and showed no sign of permeation in any of the cases tried.

DISCUSSION

Our primary aim in this work was to contrast the properties of bilayers containing either linear (C16) or branched (phytanyl) hydrophobic chains. We also wanted to determine whether ether versus ester bonding, an apparently minor structural alteration, had further biophysical implications, including the predominance of ether or ester in archaeal and eubacterial/eukaryotic lipids, respectively. Our results reveal interesting differences in the mixing properties in bilayers, interfacial polarities, nanomechanical properties of SPBs, and bilayer permeabilities to nonelectrolytes.

Regarding the lipid-mixing properties in bilayers and the formation of lipid domains, the DPhoPC/DPhPC mixed systems did not form visible domains. However, the binary mixtures of DPhoPC or DPhPC with the ester-linked DPPC did segregate into solid domains whose boundaries were highly stable, suggesting a low degree of miscibility. Combinations with DHPC also segregated into domains, but frequently showed an intermediate phase, a transient stage of lower stability and higher miscibility under the same experimental conditions (Fig. 2). After a period of ~20 min at 20°C, these transient reticulated domains broke up and formed solid ones (or were added to already present domains). We interpret this phenomenon as DHPC molecules transiting from an interdigitated ($L_\beta I$) state to a more fluid one ($P_{\beta'}$) (16). Ruocco and colleagues (27) showed that DHPC lipid bilayers are significantly thinner in this state (~3 nm), whereas DPPC ones (at the same temperature) have a thickness of ~4.4 nm. Remarkably, interdigitated membrane DPPC domains have been associated with changes in thickness described at higher temperatures (28) or after alcohol treatment (29). A reasonable explanation is to attribute the observed domains to local defects at the surface of the membrane, where some regions of the thin bilayers (rich in DHPC) are mixed with other, thicker ones (supposedly rich in branched lipids). Our observations may be related to the induction of lipid interdigitation of DPPC phases by n-butanol in DOPC/DPPC mixtures (30). Indeed, differently shaped coexisting lipid domains formed in DOPC/DPPC mixtures have been reported elsewhere in the literature (31). In such conditions, patch- and stripe-shaped gel domains in GUV bilayers were observed at different molar ratios. Interestingly, according to the DiI_{C18} fluorescence, the lipids in stripe domains were shown to be tilted. We observed a similar behavior at the equivalent molar ratio assayed in our conditions (50:50), where only patch domains were visible, whereas the reported stripe-shape domains appeared at high DPPC concentrations and could be associated with a perturbation in the plane of the membrane.

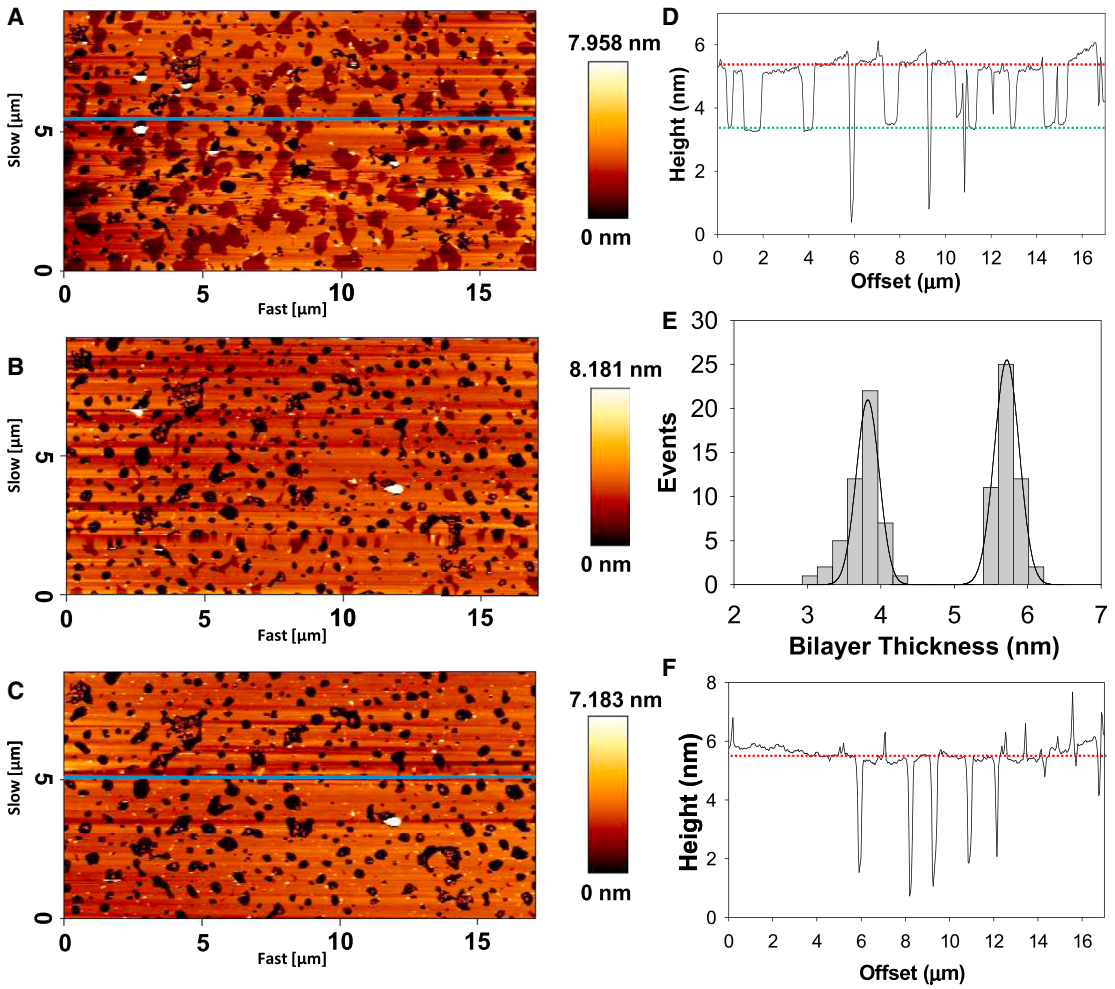

FIGURE 7 Topographic AFM analysis of DHPC SPBs. (*A–E*) Contact-mode AFM images of a DHPC supported bilayer, showing changes over time at 23°C: $t = 0$ (*A*), $t = 15$ min (*B*), and $t = 30$ min (*C*), with cross-section details from the blue lines at $t = 0$ (*D*) and $t = 30$ min (*F*), and DHPC bilayer thickness histogram as summary of the data (*E*). Black areas represent bare mica support and are used to calculate zero height as reference. Both lipid phases can be easily identified by their significantly different heights (3.82 ± 0.16 nm and 5.71 ± 0.17 nm), which are particularly clear at $t = 0$ as depicted by the dotted green and red lines (to guide the eye) in the corresponding cross section. Phase segregation disappears over time and becomes nonexistent at $t = 30$ min and only the thickest phase persists (*red dotted line* in the corresponding cross section). Thickness measurements were made by cross-section height analysis ($n = 100$) of AFM images taken from two different samples.

Nanomechanical resistance data from the four lipids gave some information about the effect of acyl-chain branching and ether linking to the glycerol backbone. Ether-linked lipids were shown to have a reduced nanomechanical resistance to AFM-tip indentation when compared with ester-linked lipids (Figs. 5 and 6). Furthermore, acyl-chain branching increased fluidity and decreased nanomechanical resistance. The combination of ether linking and acyl branching greatly enhanced this effect, and therefore the least-resistant lipid of the four under study was DPhPC. An interesting fact is that the F_b values obtained for DPhoPC were higher than expected for a fluid lipid phase in our buffer (24,32). This is in agreement with previous findings about the special properties of this lipid (e.g., water permeability) when compared with other fluid-phase lipids (17). The dual behaviors observed in both DPhoPC and DPhPC, which are unusual for other pure fluid-phase lipids in equilibrium, also argue in favor of their unique properties. DHPC, in turn, yields two distinct F_b values due to the lack of equilibrium of the system at room temperature and the metastable phase transition into an interdigitated phase (16). The coexistence of tilted gel phases and interdigitated gel phases of a pure single lipid has already been described by AFM (33), and the interdigitated gel phase exhibits a reduced thickness when compared with the tilted gel phase. This would enhance intermolecular packing and thus an increase in the F_b value would be expected. Accordingly, DHPC yields an F_b value higher than that obtained for DPPC (due to the highly packed, interdigitated phase) and another one lower than the DPPC value (due to the noninterdigitated tilted phase, weakened by ether groups).

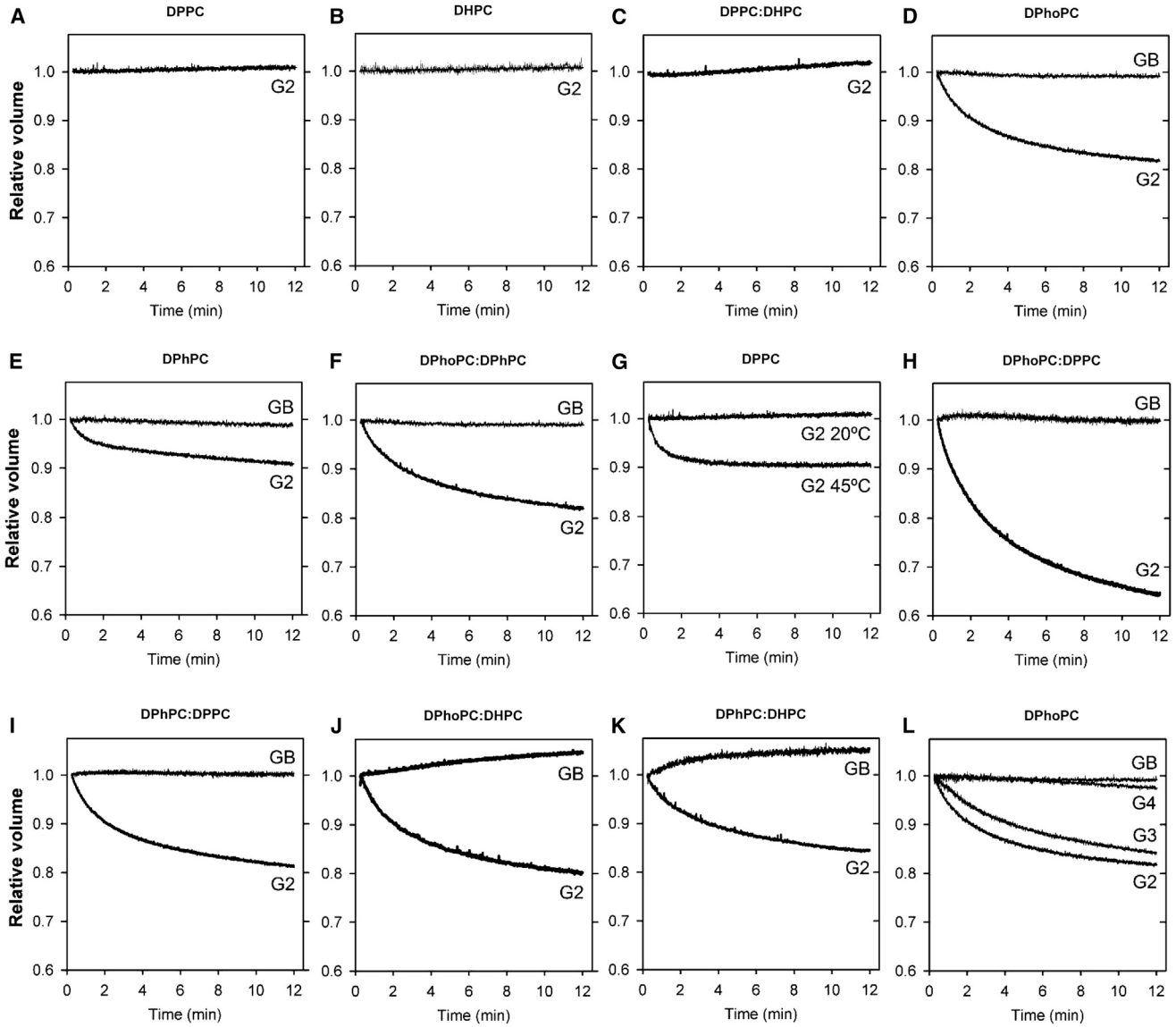

FIGURE 8 Selected kinetic profiles of polyalcohol influx through liposomes of various compositions (pure lipids or equimolecular binary mixtures). As a control, the glycine-betaine case of null permeation is included. The time-dependent decrease in absorbance at 450 nm was averaged from at least three experiments, GB, glycine-betaine; G2, ethyleneglycol; G3, glycerol; G4, erythrytol. Measurements were obtained at 20°C unless indicated otherwise.

Studies of bilayer permeability to nonelectrolytes provide a good opportunity to compare the properties of the hydrocarbon chains and polar headgroup (Table 1). When the permeability of linear-chain versus branched lipids is compared, the initial rates τ of water + e-glycol entry are higher, by ~2-fold, for the linear-chain phospholipid bilayers. Thus, at least for the four lipids under study, branching appears to make diffusion through the bilayer a less likely event. However, when the amplitude of the change in turbidity Δ, i.e., the extent of vesicle swelling, is compared, it is larger for the branched-chain bilayers. Probably, Δ and τ depend on different parameters. Specifically, the molecular areas of the branched PC are larger than those of their linear counterparts (34), and the bilayer cohesion forces, as measured by the penetration force F_b, are smaller (Figs. 5 and 6). Thus, it appears that the vesicles can swell to a larger extent when the hydrocarbon chains are branched.

Comparing ether and ester lipids is not straightforward. For linear-chain PC, ester lipids allow a faster ratio of entry (Table 1), and the ratio τ_{DPPC}/τ_{DHPC} is $\approx$ 1.2, i.e., the same value obtained for the ratio of water permeability coefficients P_{DPPC}/P_{DHPC} by Guler et al. (16). However, for the branched-chain lipids, the $\tau_{DPhoPC}/\tau_{DPhPC}$ ratio is $\approx$ 0.81, against the predictions of the previous authors. The behavior of the branched-chain lipids is not easy to understand at the moment. Nagle et al.'s (26) triple-slab theory of membrane permeability proposes that not only the hydrophobic matrix but also the two lipid/water interfaces are important for

TABLE 1 Permeabilities to e-glycol and properties of lipid vesicles in the systems under study

Mixture (1:1 mol/mol)	Linear/branched	Head-tail bond	E-glycol permeability	
			τ	Δ
DPPC (20°C)	linear	ester	—	0.00
DPPC (45°C)	linear	ester	0.43	0.08
DHPC (20°C)	linear	ether	—	0.00
DHPC (45°C)	linear	ether	0.34	0.12
DPhoPC (20°C)	branched	ester	0.15	0.17
DPhPC (20°C)	branched	ether	0.19	0.18
DPPC/DHPC (20°C)	linear/linear	ester/ether	—	0.00
DPhoPC/DPhPC (20°C)	branched/branched	ester/ether	0.13	0.18
DPhoPC/DPhPC (45°C)	branched/branched	ester/ether	0.26	0.22
DPhoPC/DPPC (20°C)	branched/linear	ester/ester	0.24	0.36
DPhoPC/DPPC (45°C)	branched/linear	ester/ester	0.41	0.18
DPhoPC/DHPC (20°C)	branched/linear	ester/ether	0.12	0.20
DPhoPC/DHPC (45°C)	branched/linear	ester/ether	0.42	0.18
DPhPC/DPPC (20°C)	branched/linear	esther/ester	0.14	0.19
DPhPC/DPPC (45°C)	branched/linear	esther/ester	0.40	0.19
DPhPC/DHPC (20°C)	branched/linear	ether/ester	0.15	0.16
DPhPC/DHPC (45°C)	branched/linear	ether/ester	0.39	0.19

In all cases, fitting of the experimental curves was done through a six-parameter exponential decay function ($f = A \times e^{-bx} + C \times e^{-dx} + G \times e^{-hx}$). In this way, we could compare the different behaviors reliably ($R^2 \geq 0.997$) in all cases. The τ-value is the slope of the curve at $t = 0$ ($A \times b + C \times d + G \times h$) and Δ is the difference in relative volume between the beginning and end of the experiments ($t = 0$ / $t = 12$ min).

permeability. We considered the properties of the ester and ether interfaces, as studied by fluorescence spectroscopy, without conclusive results (Fig. 3); for example, linear ester lipids exhibited less order (TMA-DPH) and lower hydration (Laurdan) than linear ether lipids (Fig. 4). However, these features cannot explain the slightly higher permeability of the linear ester bilayers, because for the branched lipids the opposite is true, i.e., the branched ester lipids are less ordered and less hydrated at the interface (Fig. 4), and yet they are less permeable than their ether counterparts. The possibility that other, as yet unexplored properties of the interface explain the permeability data cannot be excluded, but for the time being, the different permeabilities of ester and ether lipids remain unexplained. Note, however, that the differences in the rate and extent of permeability between ester and ether lipids are smaller than those between linear and branched lipids, suggesting that in any case the bilayer hydrophobic matrix remains the main determinant of permeability. Gawrisch et al. (35) compared DPPC and DHPC using NMR and x-ray techniques, and found that in the liquid crystalline phase the presence of carbonyl groups was not essential for lipid structure or hydration.

Finally, it is important to recall that we carried out our experiments with lipids derived from the enantiomer *sn*-glycerol-3-phosphate (*sn*-G3P), which is the glycerol moiety of bacterial/eukaryotic lipids. This facilitates the ether versus ester comparison, but does not correspond exactly to the natural lipids from *Archaea* that, apart from being ether linked, contain the *sn*-glycerol-1-phosphate isomer (*sn*-G1P) (3,36). Shimada and Yamagishi (37) used heterochiral liposomes derived from *sn*-G1P (archaea-like) and *sn*-G3P (bacterial/eukaryotic-like) lipids to determine the thermal stability of hybrid liposomes by quantification of 5-carboxyfluorescein leakage. The theoretical framework underlying this approach was to check the so-called lipid divide hypothesis (1,38,39). This conjecture relies on the assumption that mixed membranes composed of both archaeal- and bacterial/eukaryotic-type lipids could be disadvantageous for precells, causing spontaneous lipid segregation. Instead, Shimada and Yamagishi (37) demonstrated that heterochiral liposomes can be at least as stable as homochiral ones and that stability depends mainly on the lipid chain length (see also Koga (39)). Herein, we analyzed the properties of mixed liposomes derived from a single enantiomer but with different (ester or ether) headgroups, providing additional evidence for the stability of these heterogeneous lipid systems. Thus, our results support the idea that the first biomembranes could have been made of mixtures of archaeal and bacterial lipids (or close precursors) that only later segregated and were selected throughout cell evolution into bilayers of G3P-fatty acid esters and G1P-isoprenoid ethers. The present lipid divide observed in nature was possible because each lipid family could develop its own strategies or mechanisms to give membranes the necessary properties (e.g., fluidity, domain segregation, and intrinsic permeability) for biological function.

This work was supported in part by grants from the Spanish Ministerio de Ciencia e Innovación (FFI2008-06348-C02-01 to K.R.-M. and BFU2012-36241 to F.M.G.) and the University of the Basque Country (IT849-13 to F.M.G.). D.B. received support from the JAE-Transfer CSIC program and K.R.-M. received a Ramón y Cajal Research Fellowship. A.G.A. was a predoctoral student supported by the Basque Government.

REFERENCES

1. Lombard, J., P. López-García, and D. Moreira. 2012. The early evolution of lipid membranes and the three domains of life. *Nat. Rev. Microbiol.* 10:507–515.
2. Zhang, Y. M., and C. O. Rock. 2008. Membrane lipid homeostasis in bacteria. *Nat. Rev. Microbiol.* 6:222–233.
3. Chong, P. L. 2010. Archaebacterial bipolar tetraether lipids: physicochemical and membrane properties. *Chem. Phys. Lipids.* 163:253–265.
4. Peretó, J., P. López-García, and D. Moreira. 2004. Ancestral lipid biosynthesis and early membrane evolution. *Trends Biochem. Sci.* 29:469–477.
5. Rothschild, L. J., and R. L. Mancinelli. 2001. Life in extreme environments. *Nature.* 409:1092–1101.
6. Itoh, Y. H., A. Sugai, …, T. Itoh. 2001. The evolution of lipids. *Adv. Space Res.* 28:719–724.
7. Shinoda, W., M. Mikami, …, M. Hato. 2003. Molecular dynamics study on the effect of chain branching on the physical properties of lipid bilayers: structural stability. *J. Phys. Chem. B.* 107:14030–14035.
8. Greisen, Jr., P., K. Lum, …, J. A. Lundbæk. 2011. Linear rate-equilibrium relations arising from ion channel-bilayer energetic coupling. *Proc. Natl. Acad. Sci. USA.* 108:12717–12722.
9. Hsieh, C.-H., S.-C. Sue, …, W. G. Wu. 1997. Membrane packing geometry of diphytanoylphosphatidylcholine is highly sensitive to hydration: phospholipid polymorphism induced by molecular rearrangement in the headgroup region. *Biophys. J.* 73:870–877.
10. Baba, T., H. Minamikawa, …, T. Handa. 2001. Hydration and molecular motions in synthetic phytanyl-chained glycolipid vesicle membranes. *Biophys. J.* 81:3377–3386.
11. Yamauchi, K., K. Doi, …, H. Fukuda. 1992. Archaebacterial lipid models: highly salt-tolerant membranes from 1,2-diphytanylglycero-3-phosphocholine. *Biochim. Biophys. Acta.* 1110:171–177.
12. Yamauchi, K., K. Doi, …, M. Kinoshita. 1993. Archaebacterial lipids: highly proton-impermeable membranes from 1,2-diphytanyl-*sn*-glycero-3-phosphocholine. *Biochim. Biophys. Acta.* 1146:178–182.
13. Yamauchi, K., Y. Yoshida, …, M. Kinoshita. 1994. Archaebacterial lipid models: formation of stable vesicles from single isoprenoid chain-amphiphiles. *Biochim. Biophys. Acta.* 1193:41–47.
14. Yamauchi, K., K. Doi, and M. Kinoshita. 1996. Archaebacterial lipid models: stable liposomes from 1-alky1-2-phytanyl-sn-glycero-3-phosphocholines. *Biochim. Biophys. Acta.* 1283:163–169.
15. Baba, T., Y. Toshima, …, N. Kamo. 1999. Formation and characterization of planar lipid bilayer membranes from synthetic phytanyl-chained glycolipids. *Biochim. Biophys. Acta.* 1421:91–102.
16. Guler, S. D., D. D. Ghosh, …, S. Tristram-Nagle. 2009. Effects of ether vs. ester linkage on lipid bilayer structure and water permeability. *Chem. Phys. Lipids.* 160:33–44.
17. Tristram-Nagle, S., D. J. Kim, …, J. F. Nagle. 2010. Structure and water permeability of fully hydrated diphytanoylPC. *Chem. Phys. Lipids.* 163:630–637.
18. McConnell, H. M., T. H. Watts, …, A. A. Brian. 1986. Supported planar membranes in studies of cell-cell recognition in the immune system. *Biochim. Biophys. Acta.* 864:95–106.
19. Angelova, M. I., S. Soleau, …, P. Bothorel. 1992. Preparation of giant vesicles by external AC electric fields. Kinetics and applications. *Prog. Colloid Polym. Sci.* 89:127–131.
20. De Gier, J., J. G. Mandersloot, …, W. P. Van Beek. 1971. On the mechanism of non-electrolyte permeation through lipid bilayers and through biomembranes. *Biochim. Biophys. Acta.* 233:610–618.
21. Mabrey, S., and J. M. Sturtevant. 1976. Investigation of phase transitions of lipids and lipid mixtures by sensitivity differential scanning calorimetry. *Proc. Natl. Acad. Sci. USA.* 73:3862–3866.
22. Maruyama, S., H. Matsuki, …, S. Kaneshina. 1996. Thermotropic and barotropic phase behavior of dihexadecylphosphatidylcholine bilayer membrane. *Chem. Phys. Lipids.* 82:125–132.
23. Bagatolli, L. A., and E. Gratton. 2000. Two photon fluorescence microscopy of coexisting lipid domains in giant unilamellar vesicles of binary phospholipid mixtures. *Biophys. J.* 78:290–305.
24. Redondo-Morata, L., G. Oncins, and F. Sanz. 2012. Force spectroscopy reveals the effect of different ions in the nanomechanical behavior of phospholipid model membranes: the case of potassium cation. *Biophys. J.* 102:66–74.
25. Garcia-Manyes, S., L. Redondo-Morata, …, F. Sanz. 2010. Nanomechanics of lipid bilayers: heads or tails? *J. Am. Chem. Soc.* 132: 12874–12886.
26. Nagle, J. F., J. C. Mathai, …, S. Tristram-Nagle. 2008. Theory of passive permeability through lipid bilayers. *J. Gen. Physiol.* 131:77–85.
27. Ruocco, M. J., D. J. Siminovitch, and R. G. Griffin. 1985. Comparative study of the gel phases of ether- and ester-linked phosphatidylcholines. *Biochemistry.* 24:2406–2411.
28. Fang, Y., and J. Yang. 1997. The growth of bilayer defects and the induction of interdigitated domains in the lipid-loss process of supported phospholipid bilayers. *Biochim. Biophys. Acta.* 1324:309–319.
29. Mou, J., J. Yang, …, Z. Shao. 1994. Alcohol induces interdigitated domains in unilamellar phosphatidylcholine bilayers. *Biochemistry.* 33:9981–9985.
30. Kurniawan, Y., K. P. Venkataramanan, …, G. D. Bothun. 2012. *n*-Butanol partitioning and phase behavior in DPPC/DOPC membranes. *J. Phys. Chem. B.* 116:5919–5924.
31. Li, L., and J.-X. Cheng. 2006. Coexisting stripe- and patch-shaped domains in giant unilamellar vesicles. *Biochemistry.* 45:11819–11826.
32. Chiantia, S., J. Ries, …, P. Schwille. 2006. Combined AFM and two-focus SFCS study of raft-exhibiting model membranes. *ChemPhysChem.* 7:2409–2418.
33. Jiménez-Rojo, N., A. B. García-Arribas, …, F. M. Goñi. 2014. Lipid bilayers containing sphingomyelins and ceramides of varying N-acyl lengths: a glimpse into sphingolipid complexity. *Biochim. Biophys. Acta.* 1838 (1 Pt B):456–464.
34. Marsh, D. 2013. Handbook of Lipid Bilayers. CRC Press, Boca Raton, FL.
35. Gawrisch, K., D. Ruston, …, N. Fuller. 1992. Membrane dipole potentials, hydration forces, and the ordering of water at membrane surfaces. *Biophys. J.* 61:1213–1223.
36. Hung, W. C., F. Y. Chen, and H. W. Huang. 2000. Order-disorder transition in bilayers of diphytanoyl phosphatidylcholine. *Biochim. Biophys. Acta.* 1467:198–206.
37. Shimada, H., and A. Yamagishi. 2011. Stability of heterochiral hybrid membrane made of bacterial *sn*-G3P lipids and archaeal *sn*-G1P lipids. *Biochemistry.* 50:4114–4120.
38. Wächtershäuser, G. 2003. From pre-cells to Eukarya—a tale of two lipids. *Mol. Microbiol.* 47:13–22.
39. Koga, Y. 2011. Early evolution of membrane lipids: how did the lipid divide occur? *J. Mol. Evol.* 72:274–282.